



Enhanced photocatalytic activity of Bi₂O₃ under visible light irradiation by Cu(II) clusters modification



Jinli Hu^a, Hongmei Li^b, Caijin Huang^a, Min Liu^{b,c}, Xiaoqing Qiu^{a,*}

^a Research Institute of Photocatalysis, College of Chemistry and Chemical Engineering, Fuzhou University, Fuzhou 350002, China

^b Department of Information Engineering, Institute of Laser and Information, Shaoyang University, Hunan 422000, China

^c Research Center for Advanced Science and Technology, The University of Tokyo, 4-6-1 Komaba, Meguro-ku, Tokyo 153-8904, Japan

ARTICLE INFO

Article history:

Received 11 April 2013

Received in revised form 28 May 2013

Accepted 31 May 2013

Available online 8 June 2013

Keywords:

Bi₂O₃

Surface modification

Multi-electron oxygen reduction

Visible light

Photocatalyst

ABSTRACT

Using a facile hydrothermal method, pure α -Bi₂O₃ samples with rod-like structure were synthesized. Amorphous Cu(II) clusters were loaded on the as-obtained α -Bi₂O₃ samples by an impregnation method. The prepared samples were characterized by X-ray diffraction, scanning electron and transmission microscopy, X-ray photoelectron spectroscopy, and UV–visible diffuse reflectance spectroscopy. The photocatalytic activities were evaluated from gaseous 2-propanol decomposition under visible light irradiation. It is found that crystal structure and the morphologies were not changed by the Cu(II) clusters modification. Pure Bi₂O₃ sample showed a limited photocatalytic activity due to its low conduction band edge. After Cu(II) clusters modification, the photocatalytic activity was significantly improved. The Cu(II) clusters play a critical role in the charge separation and efficient oxygen reduction, which explains the enhanced photocatalytic activity.

© 2013 Elsevier B.V. All rights reserved.

1. Introduction

Since the Honda–Fujishima effect was reported [1], heterogeneous photocatalysis using semiconductors represents a very active research field due to its potential application in environmental remediation and energy conversion [2,3]. Among the semiconductor photocatalysts, TiO₂ is the most intensely investigated because of its non-toxicity, chemical stability, low cost and proper positions of the its conduction band and valence band edges. The holes produced in valence band of TiO₂ possess extremely strong oxidizing power ($E_{vb} = +2.53$ V vs standard hydrogen electrode (SHE)) toward almost all organic contaminants [4], while the conduction band level of TiO₂ is more negative than the potential for the single-electron reduction of oxygen ($O_2 + e^- = O_2^-$, $E = -0.064$ V vs SHE), facilitating consumption of photoexcited electrons by oxygen molecule [4]. Such electronic structure features make TiO₂ be an efficient photocatalyst. But the wide band gap of TiO₂ restricts its practical application, since it requires ultraviolet (UV) light for excitation. For effective utilization of the visible light that accounts for about 43% of the total solar energy, some strategies have been actively pursued to develop the “second-generation” TiO₂ based photocatalysts that can be activated by both UV and visible light, including coupling with dyes [5] or other narrow band gap

semiconductor [6,7], doping with various cations [8,9] or anions [10–12], and so on. However, these obtained photocatalysts typically show low activities. Especially, their quantum efficiencies are much lower under visible light than under UV light irradiation [13]. Thus, it appears to be urgent for us to develop novel non-TiO₂ visible light activated photocatalysts [14].

Bismuth oxide (Bi₂O₃) is an attractive material with many promising applications in electrical ceramics, solid oxide fuel cells, gas sensors, superconductors, and catalysts [15–17]. Unlike the transition metal oxides, Bi₂O₃ contains p-block Bi³⁺ ions with a formal nS^2n^0 electronic configuration that is responsible for its stereochemically activity [18]. Moreover, Bi₂O₃ has deep valence band comparable to that of TiO₂ [19]. In this respect, Bi₂O₃ is considered as a good visible light photocatalyst candidate. Unfortunately, Bi₂O₃ alone shows a very low photocatalytic activity [20], since the potential of its conduction band edge ($E_{cb} = 0.33$ V vs SHE) is not sufficient for the excited electron to reduce oxygen molecular. Even though Bi₂O₃ is widely used in composite photocatalysts, its role is a sensitizer harvesting visible light [6,21,22]. It remains as a challenging task to achieve Bi₂O₃-based photocatalysts with high photocatalytic activity under visible light irradiation. Recently, Hashimoto group reported a new effective strategy to develop visible light active photocatalysts by constructing Cu(II) or Fe(III) clusters on the surfaces of TiO₂, SrTiO₃, and WO₃ [23–27]. In these systems, it is assumed that the electrons in the valence band of the semiconductors can be transferred to the co-catalysts clusters surfaces under visible light irradiation, i.e., interfacial charge

* Corresponding author. Tel.: +81 591 83969021.

E-mail address: qiuxq@fzu.edu.cn (X. Qiu).

transfer (IFCT) [28,29], leaving holes in the valence band. The surface clusters can work as high reactive sites for oxygen reduction to scavenge the excited electrons, while the holes generated in the valence band can decompose the organic compounds, resulting in the high visible light activities [23]. Accordingly, it is expected that this methodology can be extended to some photocatalytically inactive materials, especially, low-conduction-band edge materials [26]. Having these in mind, we take Bi_2O_3 as an example to demonstrate the possibility of rational design of visible light activated photocatalysts by constructing of the oxygen reduction sites on the surface and utilizing the strong oxidizing power of holes in the deep valence band. In this work, high quality $\alpha\text{-Bi}_2\text{O}_3$ microcrystals were prepared via a hydrothermal method. After modification of Cu(II) clusters, $\text{Cu(II)-Bi}_2\text{O}_3$ shows enhanced photocatalytic activity for decomposition of gaseous 2-propanol (IPA) to CO_2 under visible light irradiation.

2. Experimental

2.1. Preparation of $\alpha\text{-Bi}_2\text{O}_3$ microcrystals

$\text{Bi(NO}_3)_3 \cdot 5\text{H}_2\text{O}$, and NaOH were used as the starting materials. The reagents were analytical grade and used as received without further purification. The Bi_2O_3 samples were prepared by a facile one-step hydrothermal process. In a typical hydrothermal synthesis procedure, 0.01 mol of $\text{Bi(NO}_3)_3 \cdot 5\text{H}_2\text{O}$ and 0.1 mol of NaOH were dissolved into 35 mL distilled water, respectively. Then the clear NaOH solution was added into BiNO_3 solution with stirring to form a yellow suspension. The suspension was transferred to a 100 mL Teflon-lined stainless steel autoclave. The autoclave was treated at 120°C for 6 h. After hydrothermal treatment, the autoclave was cooled naturally to room temperature in air. The samples were then collected by pressure filtration, washed with distilled water several times, and dried in air at ambient temperature.

2.2. Modification of $\alpha\text{-Bi}_2\text{O}_3$ microcrystals with Cu(II) clusters

The constructing of Cu(II) clusters onto the surfaces of Bi_2O_3 microcrystals was performed by an impregnation method that was described in detail in our previous works [26,30]. $\text{CuCl}_2 \cdot 2\text{H}_2\text{O}$ was used as the Cu(II) source for the modification. Briefly, 1 g of Bi_2O_3 sample was dispersed into 10 mL of CuCl_2 solution in a vial reactor. The concentration of $\text{CuCl}_2 \cdot 2\text{H}_2\text{O}$ was set to be 0.268 g/L. The sealed vial reactor was heated at 90°C for 1 h with stirring. The suspension was then filtered and washed with a sufficient amount of distilled water. The resulting residues were dried at 110°C and subsequently ground into a fine powder using an agate mortar. The sample was denoted as $\text{Cu(II)-Bi}_2\text{O}_3$.

2.3. Sample characterization

The crystal structures of the prepared powders were identified using a Rigaku MinFlex II benchtop X-ray diffractometry with $\text{Cu-K}\alpha$ irradiation. The morphologies of the samples were investigated by a field-emission scanning electron microscopy (SEM) using a JEOL JSM 2010 instrument and transition electron microscopy (TEM) on a Hitachi HF-2000 instrument under an acceleration voltage of 200 kV. UV–visible absorption spectra were obtained by the diffuse reflection method using a Lambda 900 UV/vis spectrophotometer. The chemical states of the compositional elements were studied by X-ray photoelectron spectroscopy (XPS, Perkin-Elmer model 5600). The C1s signal was used to correct the charge effects.

2.4. Photocatalytic activity test

Xenon lamp (Luminar Ace 210, Hayashi Tokei Works) with glass filters (B-47, L-42, C-40C, AGC Techno Glass) was used as a visible light source (400–530 nm) to trigger the photocatalytic reaction. The light intensity was determined by a spectroradiometer (USR-40D, Ushio) and set to be 1 mW/cm^2 . The decomposition of gaseous 2-propanol (IPA) was chosen as a probe to evaluate the photocatalytic activities of the samples. 0.3 g of the sample was evenly spread over a 5.5 cm^2 irradiation area in a 500-mL cylindrical glass vessel which was sealed with a rubber O-ring and a quartz cover. The sealed vessel was then evacuated and filled with fresh synthetic air ($\text{N}_2/\text{O}_2 = 80\%/20\%$ with the purity of 99.9%). The pressure inside the vessel was kept at about 1 atm. 300 ppm of gaseous IPA was injected into the vessel. After injecting IPA, the vessel was kept in the dark for sufficient time to ensure the establishment of absorption/desorption equilibrium of IPA on the surfaces of the samples and was then subjected to visible light irradiation to initiate the photocatalytic reactions. During the light irradiation, 1 mL gaseous sample was periodically extracted from the reaction vessel to monitor the concentrations of IPA, acetone and CO_2 using gas chromatographs (model GC-8A, Shimadzu Co., Ltd.).

3. Results and discussion

Fig. 1 shows the X-ray diffraction (XRD) patterns of the samples obtained by the hydrothermal method and with Cu(II) clusters modification i.e., $\text{Cu(II)-Bi}_2\text{O}_3$. The sharp and strong XRD peaks demonstrated that the obtained samples were highly crystallized. The peak positions coincided well with the standard data for bulk Bi_2O_3 with monoclinic structure ($\alpha\text{-Bi}_2\text{O}_3$, a thermodynamically stable phase of Bi_2O_3 at room temperature) (JCPDS Card No. 41-1449). No peaks representing other Bi_2O_3 polymorphs, such as β -, γ -, and $\delta\text{-Bi}_2\text{O}_3$ were observed [17], suggesting the high purity of the as-obtained samples. After modification with Cu(II) clusters, besides the single phase of $\alpha\text{-Bi}_2\text{O}_3$, there are no characteristic XRD peaks associated with Cu_2O and Cu(OH)_2 in the composite sample. This result was likely due to the low crystallinity and the high dispersion of Cu(II) clusters on the Bi_2O_3 surfaces, which will be confirmed by TEM analysis. Thus, the morphologies and microstructures of the samples were studied by SEM and TEM

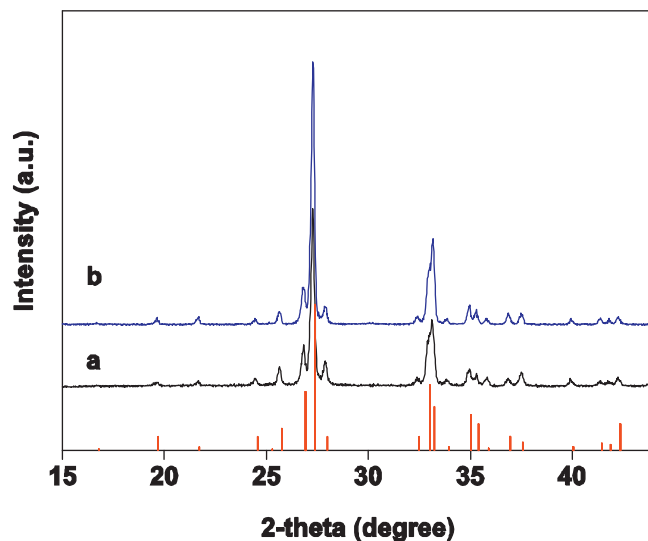


Fig. 1. X-ray diffraction patterns of samples. (a) Obtained by hydrothermal method at 120°C for 6 h and (b) modified with Cu(II) clusters. Vertical bars below the patterns represent the standard diffraction data from JCPDS file for bulk Bi_2O_3 with monoclinic structure (No. 41-1449).

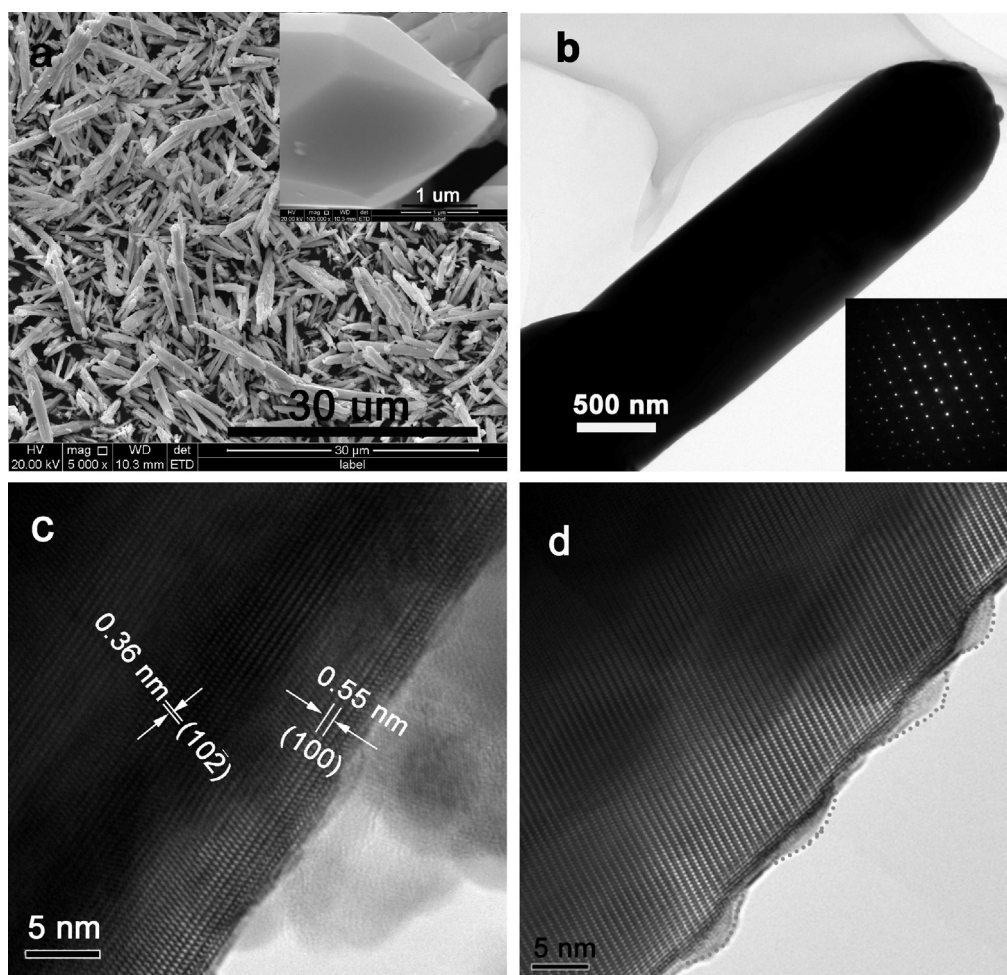


Fig. 2. (a) Typical SEM images of α - Bi_2O_3 , (b) TEM image of single α - Bi_2O_3 rod and its SAED pattern (inset), (c) HRTEM image of α - Bi_2O_3 and (d) HRTEM image of $\text{Cu(II)-Bi}_2\text{O}_3$, amorphous Cu(II) clusters were outlined by dashed line.

analysis. In a low magnification SEM image (Fig. 2a), it can be seen the α - Bi_2O_3 sample synthesized by the hydrothermal method consists of microcrystals with rod-like structures. The diameter of the rods mainly varies from 0.5 to 2 μm , and length ranges from 10 to 20 μm . A high magnification image (inset of Fig. 2a) further reveals the rod-like microcrystals possess well-defined edges, smooth surfaces and sharp tops. The morphologic characteristics of our samples were very similar to those of the α - Bi_2O_3 prepared by solution chemical method [16] and vapour transport deposition technique [31], which is possibly due to the inherent chain-type structure of Bi_2O_3 [32]. The crystal habit was further visualized by TEM observation shown in Fig. 2b. The selected area electron diffraction (SEAD) pattern is given in the inset of Fig. 2b, which demonstrated the single-crystal nature of the α - Bi_2O_3 rods. Such a crystalline structure is also confirmed the high-resolution TEM (HRTEM) images. As shown in Fig. 2c, the two-dimensional (2D) atomic lattice fringes were very clearly observed. The fringe spacing parallel to the long axis of the rod is determined to be about 0.55 nm, which is very close to the interplanar spacing of (1 0 0). The lattice fringes perpendicular to the side corresponds to the (1 0 $\bar{2}$) planes ($d=0.36$ nm) indicating the crystal growth of our α - Bi_2O_3 sample is preferential in the [1 0 $\bar{2}$] direction [16]. Interestingly, after modification, it clearly shows that some small amorphous Cu(II) clusters with the size of about 1 nm are well dispersed on the surfaces of the α - Bi_2O_3 microcrystals, as displayed in Fig. 2d. It should be mentioned that the Cu(II) clusters were hardly to be observed on the surfaces of nano SrTiO_3 , due to its small amount and good

dispersion, as reported in our previous work [26]. In this work, the particle size of α - Bi_2O_3 sample is rather large (micrometer size). This gives us the chance to directly study the deposition of Cu(II) clusters on the surfaces and evidence the good attachment of the clusters to α - Bi_2O_3 microcrystals, a property that might be beneficial for the photocatalytic activity.

XPS was used to further investigate the surface chemical status and microstructures of the samples. The binding energy values were calibrated with the C 1s signal at 284.6 eV. As shown in Fig. 3a, the high resolution XPS spectrum of Bi species in the bare sample consists of two well-resolved Bi 4f_{7/2} and Bi 4f_{5/2} photolines at 158.2 and 163.6 eV, respectively, in good agreement with the characteristic of Bi^{3+} in the α - Bi_2O_3 [6,20]. No shoulders associated with Bi^{2+} , Bi^{4+} or Bi^{5+} state in bismuth oxides was observed [33], suggesting the high purity of our sample. Furthermore, the modification of Cu(II) clusters induced negligible change of the Bi 4f spectrum, implying the only deposition of Cu(II) species on the surfaces rather than the substitution for Bi^{3+} in the lattice of α - Bi_2O_3 . Comparative studies of the Cu 2p core-level spectra of bare Bi_2O_3 and $\text{Cu(II)-Bi}_2\text{O}_3$ evidenced the existence of Cu species in the modified sample. As shown in Fig. 3b, two relatively strong main peaks at 932.9 and 952.4 eV as well as the satellite peaks in the range 944–938 eV were observed, which correspond to Cu^{2+} in copper oxide [34]. Based on the XPS analysis, the amount of Cu was roughly determined to be 0.12 wt%, nearly equal to the starting ratio used in the preparation (the weight fraction of Cu^{2+} relative to Bi_2O_3 was set to be 0.01 wt%).

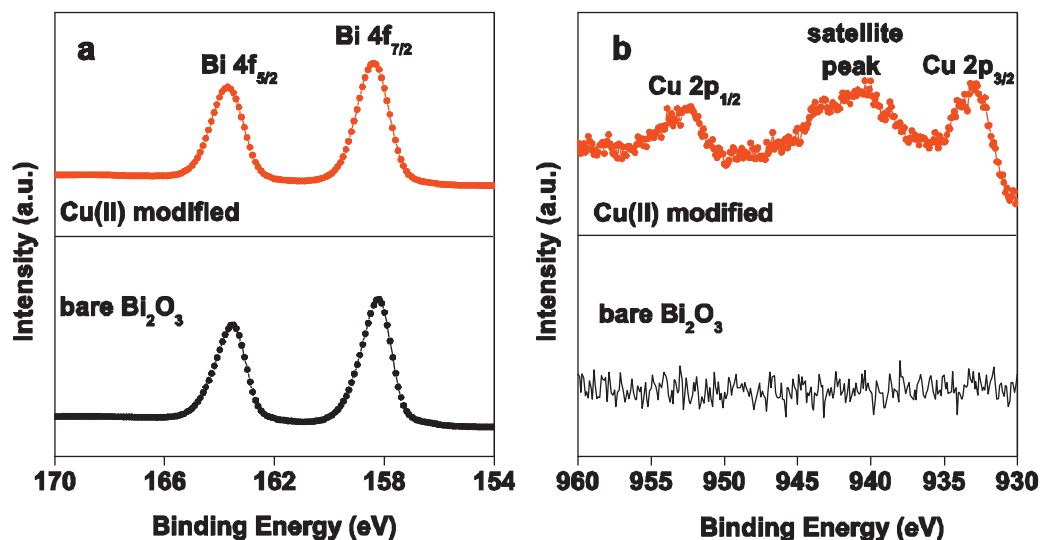


Fig. 3. (a) Bi 4f core-level spectra of bare α - Bi_2O_3 and $\text{Cu(II)-Bi}_2\text{O}_3$ and (b) Cu 2p core-level spectra of bare α - Bi_2O_3 and $\text{Cu(II)-Bi}_2\text{O}_3$.

Optical absorption properties of the semiconductor photocatalysts play an important role in the photocatalytic activity. Thus, the UV–visible absorption spectra of the samples were measured by diffuse reflectance spectroscopy at room temperature. As shown in Fig. 4, the as-obtained α - Bi_2O_3 samples exhibit a good absorption property from the UV light to visible light region. The steep shape of the spectrum at about 440 nm indicates that the visible light absorption comes from the intrinsic band gap transition of Bi_2O_3 microcrystals instead of the transition from the impurity level in the semiconductor [35]. Bi_2O_3 belongs to direct semiconductor group. For a direct band gap semiconductor, the band gap energy can be calculated by the equation: $(ah\nu)^2 = A(h\nu - E_g)$, where A is a constant, $h\nu$ is the photon energy, a is the absorption coefficient, and E_g is the band gap energy for direct transitions [36]. The E_g was thus determined to be 2.8 eV, a value that is compatible to those of bulk α - Bi_2O_3 reported in the literature [32], by extrapolating the straight portion of $(ah\nu)^2$ versus $h\nu$ plot to $(ah\nu)^2 = 0$ (inset of Fig. 4). As illustrated in Fig. 4, after Cu(II) clusters modification, besides the intrinsic band to band transition of Bi_2O_3 , $\text{Cu(II)-Bi}_2\text{O}_3$ shows two additional absorption bands in the ranges 440–500 nm and 600–800 nm. The additional absorption band in

440–500 nm results from the interfacial charge transfer from the valence band of Bi_2O_3 to Cu(II) clusters [23]. The absorption in the range 600–800 nm is due to the d – d transition of Cu(II) clusters [37].

Following the above discussion, it is imperative to investigate the effect of Cu(II) clusters modification on the photocatalytic performance. IPA was chosen as a probe to evaluate the photocatalytic activities of the samples. In order to eliminate the sample surface organic contaminants during the sample preparation and storage, the photocatalysts were fully pre-illuminated with a Xe lamp before the photocatalytic reaction. It is well known that IPA first oxidizes into acetone, an intermediate, and then finally mineralizes to CO_2 [38]. Therefore, the photocatalytic activities of the samples can be evaluated by monitoring the acetone and CO_2 concentrations. Fig. 5a describes the acetone and CO_2 evolutions from IPA decomposition over bare α - Bi_2O_3 under visible light irradiation. The removal of IPA over bare α - Bi_2O_3 is a time-consuming process. The concentration of IPA gradually decreased on prolonging the illumination time. Meanwhile, the concentration of acetone increased, accompanying the generation of small amount of CO_2 . No evident decrease of the acetone concentration was observed even after 400 h irradiation. That is, the acetone was the main product from IPA degradation instead of CO_2 , demonstrating the low photocatalytic activity of bare Bi_2O_3 . We also compared the photocatalytic activities of our samples with that of commercial TiO_2 (MT-150A, TAYCA Corp.) under the identical experimental conditions. It should be noted here that the photocatalytic performance of MT-150A is very low under visible light irradiation. Thus, the commercial TiO_2 was subjected to heat treatment at 950°C for 3 h [25]. Because the band gap of the calcined TiO_2 is about 3.0 eV, it can partially absorb incident light (400–530 nm) and exhibits visible-light photocatalytic activity to a certain extent [25]. As shown in the inset of Fig. 5a, the gas evolution phenomena over bare TiO_2 are quite similar to those over bare Bi_2O_3 . Very encouragingly, after Cu(II) clusters modification, $\text{Cu(II)-Bi}_2\text{O}_3$ exhibits enhanced photocatalytic activity compared with bare Bi_2O_3 . As shown in Fig. 5b, with the onset of visible light irradiation, the amount of IPA decreased very quickly. Complete removal of IPA was achieved after 40 h irradiation. The concentration of acetone firstly increased sharply and then decreased slowly. As a result, the amount of CO_2 , the complete degradation product of IPA, increased with the irradiation time. After 150 h irradiation, CO_2 became the main degradation product over $\text{Cu(II)-Bi}_2\text{O}_3$ photocatalyst, suggesting that Cu(II) cluster modification could improve the visible

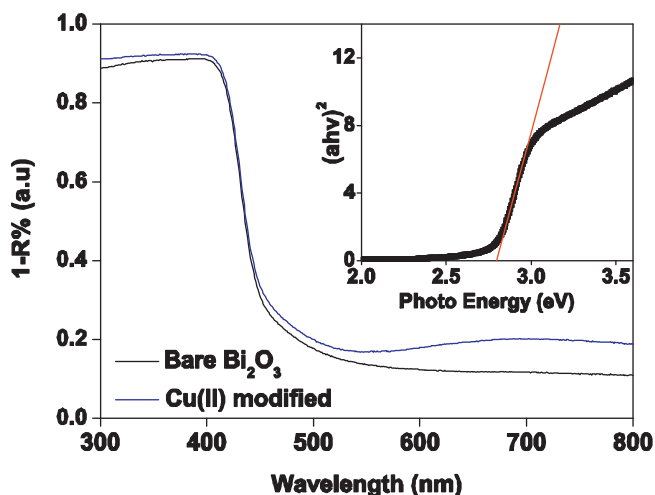


Fig. 4. UV–vis spectra of bare α - Bi_2O_3 and $\text{Cu(II)-Bi}_2\text{O}_3$, inset: Plots of $(ah\nu)^2$ vs photon energy of Bi_2O_3 .

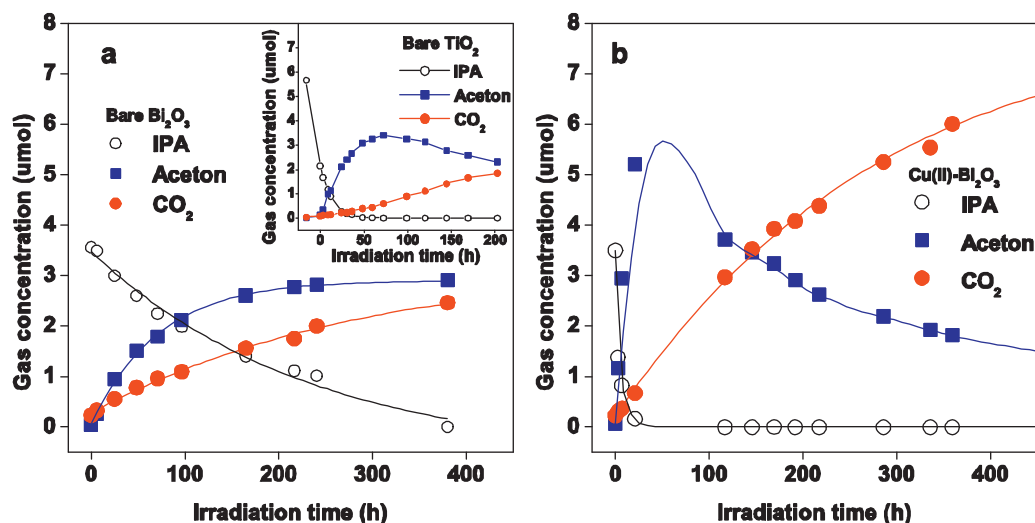


Fig. 5. Time course of CO₂ and acetone evolution from IPA decomposition under visible light irradiation (400–530 nm) over various photocatalysts, (a) bare α -Bi₂O₃, the inset of (a) displays the time-dependent gas concentrations over bare TiO₂ (MT-150A calcined at 950 °C for 3 h) under identical condition [25] and (b) Cu(II)-Bi₂O₃.

light photocatalytic performance. The trend of the gas evolutions is similar to those observed in the Cu(II)-TiO₂, and Cu(II)-SrTiO₃ codoped with Mo⁶⁺ and Na⁺ systems [23,26]. As described in Section 1, the potential of conduction band edge of Bi₂O₃ is not enough for the oxygen reduction, which explains the low photocatalytic activity of bare Bi₂O₃. In order to overcome this drawback, some noble metal nanoparticles were selected to deposit on the Bi₂O₃, wherein the noble metal nanoparticles can provide the plasmon-induced charges and serve as oxygen reduction sites [19,20,39]. In our study, it is believed that the surface Cu(II) clusters modification is responsible for the enhanced photocatalytic performance. Under visible light irradiation, the holes in the valance band can be produced by both the direct electron excitation into the conduction band and the electron transfer to Cu(II) clusters by IFCT. The excited electrons in the conduction band were then transferred to the surface Cu(II) clusters, making the efficiently charge separation. Some parts of Cu(II) clusters were subsequently turned into Cu(I). Due to the potential of Cu²⁺/Cu⁺ = 0.16 V vs SHE, the generated Cu(I) clusters can reduce the absorbed oxygen molecules via a multi-electron reduction process, and return to Cu(II) clusters [40]. On the other hand, the photoinduced holes oxidize the organic compounds due to their strong oxidation power. Consequently, enhanced photocatalytic activity was achieved over Cu(II)-Bi₂O₃ sample.

4. Conclusion

In conclusion, pure α -Bi₂O₃ samples were synthesized via a facile one-step hydrothermal method. The samples consist of rod-like α -Bi₂O₃ microcrystals with well defined edges, smooth surfaces and sharp tops. Although the pure α -Bi₂O₃ exhibited high optical absorption in the visible light range, its photocatalytic activity for IPA decomposition was rather low under visible light irradiation. By an impregnation method, amorphous Cu(II) clusters with the size of about 1 nm were well dispersed on the surfaces of α -Bi₂O₃ microcrystals. The Cu(II) clusters deposition did not change the shape and crystal structure of Bi₂O₃. Encouragingly, after Cu(II) clusters modification, enhanced photocatalytic activity was obviously observed over Cu(II)-Bi₂O₃ samples. The Cu(II) clusters can play an important role in the charge separation, and serve as reactive sites for oxygen reduction to scavenge the excited electrons, thereby improving the photocatalytic performance in combination with the strong oxidizing power holes in the valance band. This study demonstrates that the methodology of the surface

metal ion clusters modification can be extendedly employed in narrow band gap semiconductors and provides some useful guidelines for the rational design of visible light photocatalysts based on the deep valance band materials.

Acknowledgments

This work was financially supported by the National Natural Science Foundation of China (NSFC, Grant No. 21273038) and National Basic Research Program of China (973 Program) (2013CB632405).

References

- [1] A. Fujishima, K. Honda, *Nature* 238 (1972) 37–38.
- [2] X.B. Chen, C. Li, M. Grätzel, R. Kostecki, S.S. Mao, *Chemical Society Reviews* 41 (2012) 7909–7937.
- [3] H. Tong, S.X. Ouyang, Y.P. Bi, N. Umezawa, M. Oshikiri, J.H. Ye, *Advanced Materials* 24 (2012) 229–251.
- [4] K. Hashimoto, H. Irie, A. Fujishima, *Japanese Journal of Applied Physics* 44 (2005) 8269–8285.
- [5] C.C. Chen, W.H. Ma, J.C. Zhao, *Chemical Society Reviews* 39 (2010) 4206–4219.
- [6] Z.F. Bian, J. Zhu, S.H. Wang, Y. Cao, X.F. Qian, H.X. Li, *Journal of Physical Chemistry C* 112 (2008) 6258–6262.
- [7] Y. Bessekhouad, D. Robert, J.V. Weber, *Catalysis Today* 101 (2005) 315–321.
- [8] M. Mrowetz, W. Balcerski, A.J. Colussi, M.R. Hoffmann, *Journal of Physical Chemistry B* 108 (2004) 17269–17273.
- [9] X. Chen, S.S. Mao, *Chemical Reviews* 107 (2007) 2891–2959.
- [10] R. Asahi, T. Morikawa, T. Ohwaki, K. Aoki, Y. Taga, *Science* 293 (2001) 269–271.
- [11] S.U.M. Khan, M. Al-Shahry, W.B. Ingler, *Science* 297 (2002) 2243–2245.
- [12] S. Sakthivel, H. Kisch, *Angewandte Chemie International Edition* 42 (2003) 4908–4911.
- [13] H. Irie, Y. Watanabe, K. Hashimoto, *Journal of Physical Chemistry B* 107 (2003) 5483–5486.
- [14] L.W. Zhang, Y.F. Zhu, *Catalysis Science & Technology* 2 (2012) 694–706.
- [15] A. Hameed, T. Montini, V. Gombac, P. Fornasiero, *Journal of the American Chemical Society* 130 (2008) 9658–9659.
- [16] X.L. Gou, R. Li, G.X. Wang, Z.X. Chen, D. Wexler, *Nanotechnology* 20 (2009) 495501.
- [17] P. Shuk, H.D. Wiemhöfer, U. Guth, W. Göpel, M. Greenblatt, *Solid State Ionics* 89 (1996) 179–196.
- [18] A. Walsh, G.W. Watson, D.J. Payne, R.G. Edgell, J. Guo, P.A. Glans, T. Learmonth, K.E. Smith, *Physical Review B* 73 (2006) 235104.
- [19] R.H. Li, W.X. Chen, H. Kobayashi, C.H. Ma, *Green Chemistry* 12 (2010) 212–215.
- [20] H.Y. Jiang, K. Cheng, J. Lin, *Physical Chemistry Chemical Physics* 14 (2012) 12114–12121.
- [21] X. Zhao, H.J. Liu, J.H. Qu, *Applied Surface Science* 257 (2011) 4621–4624.
- [22] S. Balachandran, M. Swaminathan, *Journal of Physical Chemistry C* 116 (2012) 26306–26312.
- [23] H. Irie, S. Miura, K. Kamiya, K. Hashimoto, *Chemical Physics Letters* 457 (2008) 202–205.
- [24] H.G. Yu, H. Irie, K. Hashimoto, *Journal of the American Chemical Society* 132 (2010) 6898–6899.

- [25] H.G. Yu, H. Irie, Y. Shimodaira, Y. Hosogi, Y. Kuroda, M. Miyauchi, K. Hashimoto, *Journal of Physical Chemistry C* 114 (2010) 16481–16487.
- [26] X.Q. Qiu, M. Miyauchi, H.G. Yu, H. Irie, K. Hashimoto, *Journal of the American Chemical Society* 132 (2010) 15259–15267.
- [27] X.Q. Qiu, M. Miyauchi, K. Sunada, M. Minoshima, M. Liu, Y. Lu, D. Li, Y. Shimodaira, Y. Hosogi, Y. Kuroda, K. Hashimoto, *ACS Nano* 6 (2012) 1609–1618.
- [28] C. Creutz, B.S. Brunschwig, N. Sutin, *Journal of Physical Chemistry B* 109 (2005) 10251–10260.
- [29] C. Creutz, B.S. Brunschwig, N. Sutin, *Journal of Physical Chemistry B* 110 (2006) 25181–25190.
- [30] M. Liu, X.Q. Qiu, M. Miyauchi, K. Hashimoto, *Chemistry of Materials* 23 (2011) 5282–5286.
- [31] Y.F. Qiu, M.L. Yang, H.B. Fan, Y.Z. Zuo, Y.Y. Shao, Y.J. Xu, X.X. Yang, S.H. Yang, *CrystEngComm* 13 (2011) 1843–1850.
- [32] S. Anandan, G.J. Lee, P.K. Chen, C.H. Fan, J.J. Wu, *Industrial and Engineering Chemistry Research* 49 (2010) 9729–9737.
- [33] D. Barreca, F. Morazzoni, G.A. Rizzi, R. Scotti, E. Tondello, *Physical Chemistry Chemical Physics* 3 (2001) 1743–1749.
- [34] L. Huang, F. Peng, F.S. Ohuchi, *Surface Science* 603 (2009) 2825–2834.
- [35] X.Q. Qiu, G.S. Li, X.F. Sun, L.P. Li, X.Z. Fu, *Nanotechnology* 19 (2008) 215703.
- [36] X.Q. Qiu, L.P. Li, J. Zheng, J.J. Liu, X.F. Sun, G.S. Li, *Journal of Physical Chemistry C* 112 (2008) 12242–12248.
- [37] N.L.D. Filho, *Mikrochimica Acta* 130 (1999) 233–240.
- [38] Y. Ohko, K. Hashimoto, A. Fujishima, *Journal of Physical Chemistry A* 101 (1997) 8057–8062.
- [39] Z.L. Xu, I. Tabata, K. Hirogaki, K. Hisada, T. Wang, S. Wang, T. Hori, *RSC Advances* 2 (2012) 103–106.
- [40] Y. Nosaka, S. Takahashi, Y. Mitani, X.Q. Qiu, M. Miyauchi, *Applied Catalysis B* 111/112 (2012) 636–640.